ated interdigital piezoelectric transducers," *IEEE Trans. Sonics Ultrason.*, vol. SU-19, no. 4, p. 448, July 1972.
[6] T. I. Browning, M. F. Lewis, and R. F. Milson "Surface acoustic waves on rotated *Y*-cut $LiTaO_3$," in *Proc. 1978 Ultrason. Symp.*, p. 586.
[7] C. O. Newton, "Transducer and multistrip coupler performance for leaky surface waves on lithium niobate," *Elect. Lett.*, vol. 9, no. 21, p. 481, 1973.
[8] K. Yamaroushi and K. Shibayama, "Propagation and amplification of Rayleigh waves and piezoelectric leaky surface waves in $LiNbO_3$," *J. Appl. Phys.*, vol. 43, p. 856, 1972.
[9] P. D. Bloch, N. G. Doe, E. G. S. Paige, and M. Yamaguchi "Observations of surface skimming bulk waves and other waves launched from an IDT on lithium niobate," in *Proc. 1981 Ultrason. Symp.*, p. 268.
[10] F. G. Marshall, C. O. Newton, and E. G. S. Paige, "Theory and design of the surface acoustic wave multistrip coupler," *IEEE Trans. Sonics Ultrason.*, vol. SU-20, no. 2, p. 124, Mar. 1973.

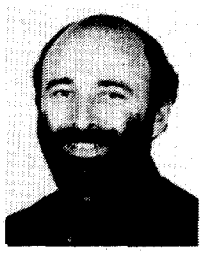

Paul D. Bloch (M'83) was born in Bridgend, Wales, on March 1, 1951. He received the B.A. degree in physics and the D.Phil. degree in solid-state physics from the University of Oxford, Oxford, England, in 1972 and 1977, respectively.

He was Royal Society European Fellow at the Laboratoire de Spectroscopie, Universite Louis Pasteur, Strasbourg, form 1977–1978. Since April 1978 he has been Research Fellow at the Department of Engineering Science, University of Oxford, England. His research interests include bulk and surface acoustic waves and optical holography.

Dr. Bloch is a member of the Institute of Physics.

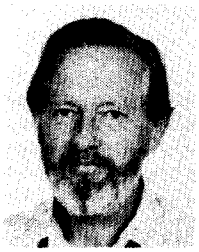

Edward G. S. Paige was born in Hastings, England, on July 18, 1930. He received the B.Sc. degree in physics and the Ph.D. degree from Reading University, Reading, England, in 1952 1955 respectively.

From 1955–1977 he was at the Royal Signal and Radar Establishment, Malvern, Worcestershire, England. There his work included transport and optical properties of semiconductors and surface acoustic wave devices and applications. In 1977 he joined the staff of the University of Oxford, Oxford, England, as Professor of Engineering in the Department of Engineering Science. His current interests include surface and bulk waves, acoustics, and optical holography.

Dr. Paige is a Fellow of the Royal Society, Fellow of the Institute of Physics, and Fellow of the Institute of Electrical Engineers.

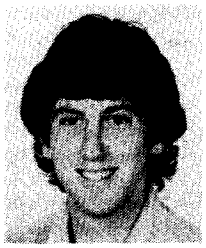

Michael W. Wagg was born in Hobart, Australia, on January 4, 1956. He received the B.Sc. and B.Eng. degrees from the University of Tasmania, Australia, in 1976 and 1978, respectively.

From 1978–81 he was Rhodes Scholar at the Department of Engineering Science, Oxford University receiving the D.Phil. degree in 1981.

He is at present working with the Overseas Telecommunications Commission, Sydney, Australia.

Quantitative Calculation and Measurement of Longitudinal and Transverse Ultrasonic Wave Pulses in Solid

KATSUHIRO KAWASHIMA, MEMBER, IEEE

Abstract—**Quantitative calculation and measurement of both longitudinal and transverse ultrasonic wave pulses in an aluminum sample generated by a vertical surface force have been made. The electromagnetic surface force generated on the metal surface by a pulse current flowing in a pancake coil was used as a quantitative standard sound source, and this force was calculated using the observed pulse current and the coil dimensions. Then, both the longitudinal and transverse wave pulses generated by this force were calculated by superimposing continuous sinusoidal ultrasonic waves given by the rigorous integral representations for the waves and were also measured by the small electromagnetic-ultrasonic transducers of a good measurement reproducibility. The calculated and measured waveforms in the time-domain corresponded excellently to each other for all the cases, including the very complicated waveforms in the case of larger angles. The quantitative discrepancy between the calculated and the measured size of the waveforms was 48 percent for the longitudinal wave pulses and 34 percent for the transverse wave pulses. This kind of quantitative comparison between the theory and the experiment has seldom been done, and the discrepancy obtained is considered to be smaller than any other results obtained. Both the theoretical and experimental methods described are useful for the quantitative evaluation of the ultrasonic wave-field in metal.**

Manuscript received January 11, 1983.

The author is with the Process Technology Research and Development Laboratory, Nippon Steel Corporation, 1-1-1 Edamitsu, Yawatahigashi, Kitahyushu, 805 Japan.

0018-9537/84/0300-0083$01.00 © 1984 IEEE

I. Introduction

QUANTITATIVE evaluation of the pulse ultrasonic wavefield in elastic medium is important not only for the fundamental elastic wave problem but also for the assessment of ultrasonic transducers and for the proper application of the ultrasonic wave technique to nondestructive testing and many other measurement methods.

Although several papers concerning this problem were reported earlier [1]-[5] the quantitative comparison between the calculation and measurement of pulse ultrasonic waveforms in the time-domain for both longitudinal and transverse ultrasonic pulses in a solid have not been done. In this paper this problem will be attacked by the following methods. First, the electromagnetic surface force generated on the surface of an aluminum sample by a flat pancake coil carrying a pulse current of a high peak intensity is used as a standard quantitative sound source in the experiment. A simple but useful formula to calculate the pulse electromagnetic surface force (rather than the sinusoidally oscillating force [3]) is derived on the ground that the electromagnetic skin depth is much smaller than the ultrasonic wavelength, and so the electromagnetic body force may be integrated with respect to the depth to obtain the electromagnetic surface force. Second, the pulse ultrasonic waves in the aluminum sample are calculated by superimposing the various sinusoidal waves calculated by the rigorous integral representations that were given earlier [6]-[8]. Third, the two types of small electromagnetic-ultrasonic transducers are made and used for individual measurements of the longitudinal and transverse ultrasonic wave pulses. The characteristics of these two transducers are theoretically analyzed, and the formula for the sensitivity of the transducers is developed, which is largely different from the earlier treatment for the sinusoidal ultrasonic waves [5]. Finally the calculated and measured ultrasonic waveforms are compared and discussed.

II. Theory

A. Pulse Electromagnetic Surface Force

The electromagnetic vector potential $A_\phi(r, z)$ inside a metal sample, which is produced by the sinusoidal currents I flowing in a flat pancake coil shown in Fig. 1 was obtained by using the same method reported earlier by Dodd and Deeds [9] and Onoe [10]

$$A_\phi(r,z) = \mu_1 \frac{NI}{r_2 - r_1} \int_0^\infty \frac{1}{\zeta^2} \int_{\zeta r_1}^{\zeta r_2} uJ_1(u)\,du\,J_1(\zeta r) \cdot e^{-\zeta h} \frac{e^{-\eta_1 z}}{\frac{\mu_1}{\mu_0} + \frac{\eta_1}{\zeta}} d\zeta, \quad (1)$$

where

η_1 $= \sqrt{\zeta^2 + j\omega\mu_1\sigma_1}$,
r_2 outside radius,
r_1 inside radius,
h air gap between the coil and the metal surface,
μ_0, μ_1 magnetic permeability of air and metal, and
σ_1 electric conductivity of metal.

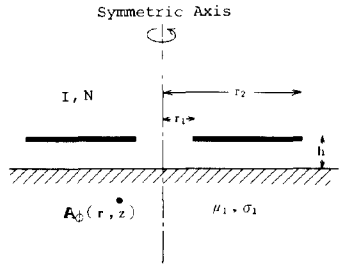

Fig. 1. Model of a flat pancake coil and a conductive half-space to calculate electromagnetic vector potential.

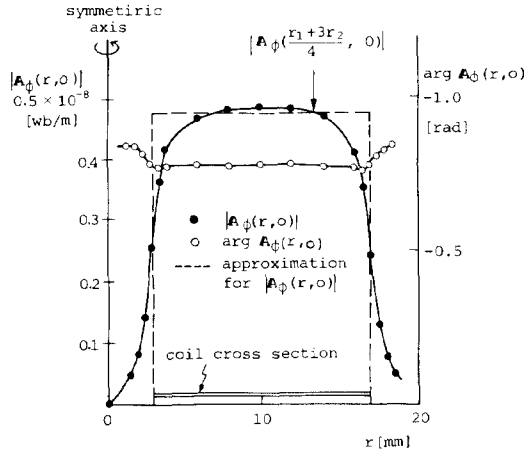

Fig. 2. Distribution of calculated vector potential $A_\phi(r, 0)$ on surface of conductive half-space beneath the coil.

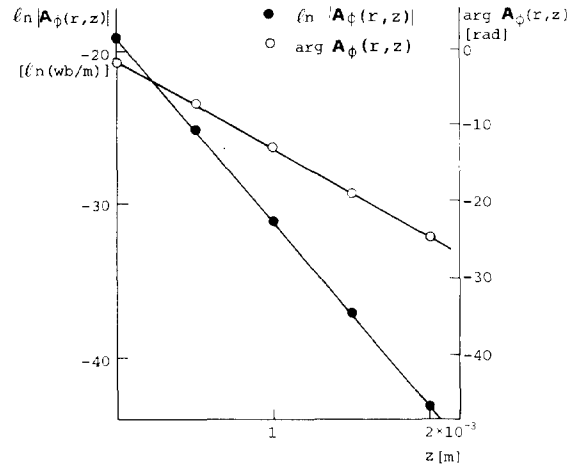

Fig. 3. Dependency on depth of calculated vector potential $A_\phi(r, z)$ at $r = 10$ mm.

Figs. 2, 3 show the calculated results of the electromagnetic vector potential at the surface and at several depths, respectively. The outside and inside radius of the coil is 17 and 0.3 mm, respectively, and the frequency of the coil current is 1 MHz. The other conditions for the calculation are shown in Table I. Fig. 2 shows that the amplitude $|A_\phi(r, z)|$ and the phase $\arg A_\phi(r, z)$ remain approximately constant within the area directly beneath the coil, and it may be assumed that the electromagnetic vector potential at any point beneath the coil, $A_\phi(r, 0)$ has approximately the same value as the one found at $r = (r_1 + 3r_2)/4$, $A_\phi((r_1 + 3r_2)/4, 0)$, as shown by the

TABLE I
CONDITIONS FOR CALCULATION OF VECTOR POTENTIAL SHOWN IN FIGS. 2, 3

Coil Conditions				Current		Metal	
outside radius	inside radius	air gap.	number of turns	amplitude	frequency	permeability	conductivity
3 mm	17 mm	0.6 mm	1	1 A	1 MHz	$4\pi \times 10^{-7}$ H/m	3.65×10^{7} Mho/m

broken line in Fig. 2. Fig. 3 shows that the dependency of the vector potential on the depth z is approximately the same as that of the electromagnetic plane wave. The results mentioned above allow the following approximate formula for the vector potential

$$A_\phi(r, z) \doteqdot A_\phi\left(\frac{r_1 + 3r_2}{4}, z\right) \doteqdot A_\phi\left(\frac{r_1 + 3r_2}{4}, 0\right) e^{-(1+j)z/\delta}, \tag{2}$$

where

$$\delta = \sqrt{\frac{2}{\omega \mu_1 \sigma_1}}.$$

Eq. (1) was also calculated for other various combinations of different conditions, five different coil sizes $(r_1 - r_2)$ 6 mm ~ 18 mm, four different air gaps, h 0.2 mm ~ 3.0 mm, seven different frequencies, 50 KHz ~ 5 MHz, and three different electric conductivity of metal, $1.33 \times 10^6 \sim 5.88 \times 10^7$ Mho/m. The calculated results indicated that the same approximation as (2) was valid for all the conditions. Those results were summarized, and the approximate formula for the vector potential was derived

$$A_\phi(r, z) \doteqdot A_\phi\left(\frac{r_1 + 3r_2}{4}, z\right) \doteqdot \mu_1 \frac{NI}{r_2 - r_1} \cdot K(r_1, r_2, h) \frac{\delta}{1+j} e^{-(1+j)z/\delta}, \tag{3}$$

where

$$K(r_1, r_2, h) = \exp\left\{-\left(\frac{1.75}{\bar{r}_2 - \bar{r}_1} + 0.5\right)\bar{h}\right\}$$

$$\bar{r}_1 = r_1/r_{12}, \bar{h} = h/r_{12}$$

$$\bar{r}_2 = r_2/r_{12}, r_{12} = (r_1 + r_2)/2.$$

The approximation error of (3) is smaller than 5 percent under the condition, $h < 0.3\,(r_2 - r_1)$.

A pulse current $I_P(t)$ which is given by the following Fourier integral is supplied to a pancake coil

$$I_P(t) = \frac{1}{\pi} \mathrm{Re} \int_0^\infty I e^{j\omega t}\, d\omega, \tag{4}$$

where

$$I = \int_{-\infty}^{\infty} I_P(t)\, e^{-j\omega t}\, dt. \tag{5}$$

A pulse electromagnetic body force per-unit metal volume $F_P(r, z, t)$ is given by the eddy current density $J_P(r, z, t)$ and the magnetic flux density $B_P(r, z, t)$

$$F_P(r, z, t) = J_P(r, z, t)\, B_P(r, z, t). \tag{6}$$

If $I_P(t)$ is a short pulse current and the principal frequency of it is high, $F_P(r, z, t)$ is generated only at the shallow depths and may be integrated with respect to depth z to produce a pulse surface force $P_P(r, t)$

$$P_P(r, t) = \int_{-\infty}^{0} F_P(r, z, t)\, dz = \int_{-\infty}^{0} J_P(r, z, t)\, B_P(r, z, t)\, dz = \int_{-\infty}^{0} \sigma_1 \frac{\partial A_P(r, z, t)}{\partial t} \frac{\partial A_P(r, z, t)}{\partial z}\, dz. \tag{7}$$

$A_P(r, z, t)$ is the electromagnetic vector potential produced by the pulse current $I_P(t)$ and is given by

$$A_P(r, z, t) = \frac{1}{\pi} \mathrm{Re} \int_0^\infty A_\phi(r, z)\, e^{j\omega t}\, d\omega. \tag{8}$$

Substituting (3), (5), (8) into (7) gives

$$P_P(t) \equiv P_P\left(\frac{r_1 + 3r_2}{4}, t\right) \doteqdot \sigma_1 \left\{\frac{\mu_1 N}{r_2 - r_1} K(r_1, r_2, h)\right\}^2 \frac{1}{\pi^2} \cdot \int_{-\infty}^{0} \left\{ \mathrm{Re} \int_0^\infty \left(I \frac{\delta}{1+j} e^{(1+j)z/\delta}\, j\omega e^{j\omega t}\right) d\omega \cdot \mathrm{Re} \int_0^\infty \left(I e^{(1+j)z/\delta}\, e^{j\omega t}\right) d\omega \right\} dz. \tag{9}$$

Simplifying (9) gives

$$P_P(t) \equiv P_P\left(\frac{r_1 + 3r_2}{4}, t\right) = \frac{1}{2}\mu_1 \left\{\frac{N}{r_2 - r_1} K(r_1, r_2, h)\right\}^2 \cdot \frac{1}{\pi^2} \left\{ \mathrm{Re} \int_0^\infty I e^{j\omega t}\, d\omega \right\}^2 = \frac{1}{2}\mu_1 \left\{\frac{N}{r_2 - r_1} K(r_1, r_2, h)\right\}^2 \{I_P(t)\}^2. \tag{10}$$

Eq. (10), which has not been self-evident, is simple but useful. We can approximately calculate a pulse electromagnetic surface force working vertically to the metal surface within the circular area beneath the coil by using the square of a pulse current $\{I_P(t)\}^2$ and the other known conditions of the coil and metal. It is worth noting that the electrical conductivity σ_1 has nothing to do with the surface force because it has vanished through integration of the body force with respect to depth.

A formula similar to (10) was obtained earlier [11], but it

was only for the condition that a coil and a metal membrane in close mechanical contact in water and it was quantitatively different from (10).

B. Pulse Ultrasonic Wave Generated by a Pulse Surface Force

Sinusoidal ultrasonic waves are generated in a semi-infinite elastic half-space by a sinusoidally oscillating unit force working vertically to the surface within a circular area of radius a_1. The rigorous integral representations for the displacement amplitudes at an arbitrary point have been given by Nakano [6], Miller and Pursey [7], and [8], each using different mathematical methods

$$\boldsymbol{S}_z \equiv \boldsymbol{S}_z(r,z) = \frac{a_1}{\mu}\int_0^\infty \frac{\alpha_1}{f_0(\alpha)}\left[(\kappa^2 - 2\alpha^2)\exp(-\alpha_1 z) + 2\alpha^2 \exp(-\alpha_\kappa z)\right] J_0(\alpha r) J_1(\alpha a_1)\, d\alpha, \tag{11}$$

$$\boldsymbol{S}_r \equiv \boldsymbol{S}_r(r,z) = \frac{a_1}{\mu}\int_0^\infty \frac{\alpha}{f_0(\alpha)}\left[(\kappa^2 - 2\alpha^2)\exp(-\alpha_1 z) + 2\alpha_1\alpha_\kappa \exp(-\alpha_\kappa z)\right] J_1(\alpha r) J_1(\alpha a_1)\, d\alpha, \tag{12}$$

where

$$f_0(\alpha) = (2\alpha^2 - \kappa^2)^2 - 4\alpha^2\alpha_1\alpha_\kappa$$

$$\alpha_1 = (\alpha^2 - 1)^{1/2}, \quad \alpha_\kappa = (\alpha^2 - \kappa^2)^{1/2}, \quad \kappa^2 = \kappa_S^2/\kappa_C^2$$

$$\kappa_C^2 = \rho\omega^2/(\lambda + 2\mu), \quad \kappa_S^2 = \rho\omega^2/\mu$$

λ, μ Lame constants.

$\boldsymbol{S}_z$ and $\boldsymbol{S}_r$ are z- and r-components of the displacement amplitude, respectively. The pulse displacements $S_{zp}(t) \equiv S_{zp}(r,z,t)$, $S_{rp}(t) \equiv S_{rp}(r,z,t)$ generated by a pulse surface force $P_P(t)$ can be calculated by superimposing the sinusoidally oscillating displacements calculated by (11), (12).

$$S_{zp}(t) = \frac{1}{\pi}\mathrm{Re}\int_0^\infty C(\omega)\,\boldsymbol{S}_z\, e^{j\omega t}\, d\omega, \tag{13}$$

$$S_{rp}(t) = \frac{1}{\pi}\mathrm{Re}\int_0^\infty C(\omega)\,\boldsymbol{S}_r\, e^{j\omega t}\, d\omega, \tag{14}$$

where

$$C(\omega) = \frac{1}{\pi}\int_{-\infty}^{\infty} P_P(t)\, e^{-j\omega t}\, d\omega.$$

The normal and tangential components of the pulse displacement $S_{np}(t) \equiv S_{np}(r,z,t)$ and $S_{tp}(t) \equiv S_{tp}(r,z,t)$ at a point on a sphere centered by the sound source are given by (See Fig. 4.)

$$S_{np}(t) = S_{zp}(t)\cos\theta + S_{rp}(t)\sin\theta, \tag{15}$$

$$S_{tp}(t) = -S_{zp}(t)\sin\theta + S_{rp}(t)\cos\theta. \tag{16}$$

Equations (11), (12) were numerically integrated along the path on the real axis which must be diverted into the complex plane to pass by the real pole. The widths of the numerical quadratures were carefully changed to follow the fluctuation of the function to be integrated. The numerically integrated results for the various frequencies were substituted into (13)-(16), and the pulse displacements $S_{np}(t)$, $S_{tp}(t)$ were obtained. Through this method the longitudinal and transverse wave components of $S_{np}(t)$ and $S_{tp}(t)$ were automatically separated in time because of the difference between the two wave velocities.

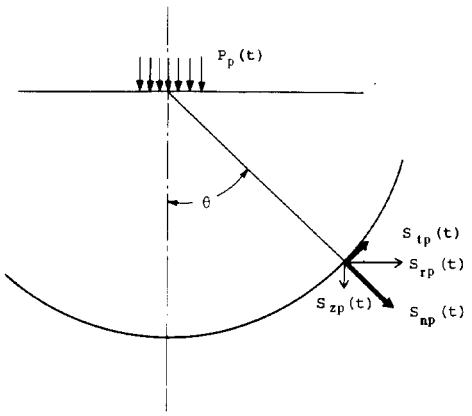

Fig. 4. Normal and tangential components of a pulse displacement produced by a pulse surface force.

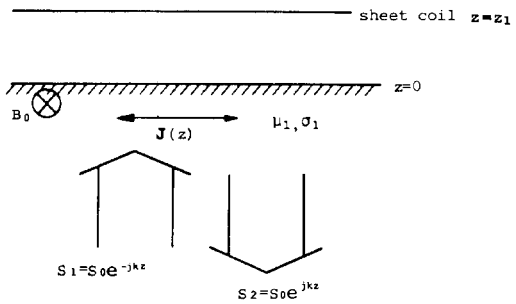

Fig. 5. One-dimensional model for theory of electromagnetic detection of ultrasonic waves in metal.

C. Detection of Ultrasonic Wave Pulses

Sinusoidally oscillating longitudinal plane ultrasonic waves $\boldsymbol{S}(z) = S_0 e^{-jk_c z}$ in the semi-infinite metal proceeds to the surface and is reflected back. (See Fig. 5.) Then the sinusoidal oscillation of metal particle $\xi(z)$ is given by the sum of both waves

$$\xi(z) = S_0(e^{-jk_c z} + e^{jk_c z}). \tag{17}$$

A stationary magnetic field B_0 is given the direction of which is perpendicular to the particle oscillation. Eddy current $\boldsymbol{J}(z)$ is induced through the interaction between B_0 and $\xi(z)$

$$\boldsymbol{J}(z) = \sigma_1 \frac{\partial \xi(z)}{\partial t} B_0 = j\omega\sigma_1 S_0(e^{-jk_c z} + e^{jk_c z}) B_0. \tag{18}$$

The vector potential $A_x(z_1)$ in the air is produced by the whole eddy current in the metal and can be easily calculated by using Maxwell's electromagnetic equation and (18)

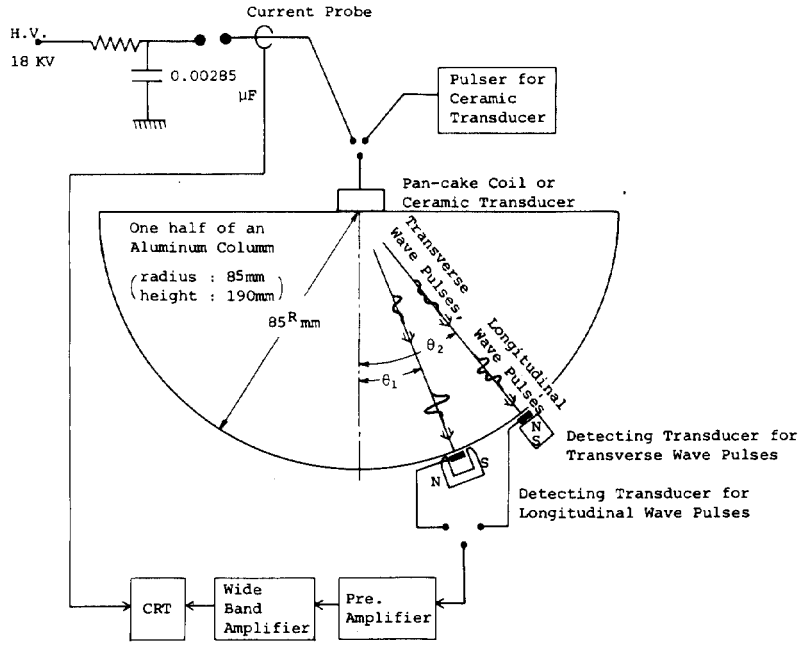

Fig. 6. Experimental arrangement for measurement of ultrasonic pulses in metal.

$$A_x(z_1) = 2S_0B_0 \frac{1}{1 - j\frac{1}{2}k_c^2\delta^2}. \tag{19}$$

Then the induced voltage in a rectangular area $W(=a \times b)$ within a sheet coil that consists of the strait wires and extends over the metal is given by

$$\begin{aligned} V &= N_x abE \\ &= -N_x Wj\omega A_x(z_1) \\ &= -N_x Wj\omega 2S_0B_0 \frac{1}{1 - j\frac{1}{2}k_c^2\delta^2}, \end{aligned} \tag{20}$$

where

N_x number of wires per meter,
k_c wavenumber of ultrasonic waves, and
δ electromagnetic skin depth.

In the case of a pulse ultrasonic wave $S_p(t, z)$, a pulse voltage $V_p(t)$ is obtained by neglecting the small value $\frac{1}{2}k_c^2\delta^2$ and replacing $j\omega$ with $\partial/\partial t$, because no ω is contained in (20) except $j\omega$ after $\frac{1}{2}k_c^2\delta^2$ is neglected

$$V_p(t) = -N_x WB_0 \frac{\partial}{\partial t}(2S_p(t, 0)). \tag{21}$$

Eq. (21) also holds for the transverse ultrasonic wave as shown by only changing the directions of the metal particle oscillation and the magnetic flux, and then following the same mathematical procedure. Eq. (21) is important and useful, because the pulse voltage can be obtained simply by differentiation with respect to the time of a pulse displacement amplitude at the surface, $2S_p(t, 0)$. Simple consideration might only lead to a wrong conclusion that the voltage pulse should be proportional to the second differentiation of the displacement amplitude with respect to time, because according to the fundamental electromagnetic theory, the induced voltage is proportional to the differentiation of the magnetic flux, which is proportional to the induced current in the metal, and the induced current is proportional to the differentiation of the displacement amplitude with respect to time. This is true only in the case where the displacement amplitude of ultrasonic waves exists only at a certain depth. As a result of the integration with respect to depth, the first differentiation with respect to time has just formally been cancelled.

III. Experiment

A. Experimental Method

The experimental arrangement for the measurement is shown in Fig. 6. To generate a pulse electromagnetic surface force as a ultrasonic wave source, a flat pancake coil was placed on the flat side of an aluminum sample, shown in Fig. 7; and a spark gap was used to discharge a capacitance (0.00285 μF) to make a pulse current of the high peak intensity. The outside and the inside radius of the coil was 10 mm and 1.7 mm respectively, the diameter of the wire, including the insulator was 0.39 mm, the number of turns wound in a single layer was 18, and the air gap or the distance between the metal surface and the center of the wire was 0.435 mm. (See Fig. 7 and 8.) The coil current was measured by a wide-band current probe (Model 411: Pearson Electronics) and the measured current waveform is shown in Fig. 9, which is represented by

$$I_p(t) = I_0 e^{-\alpha t} \sin \beta t, \tag{22}$$

where

I_0 1500 A,
α 6.76×10^5 1/s,
β 5.93×10^6 1/s.

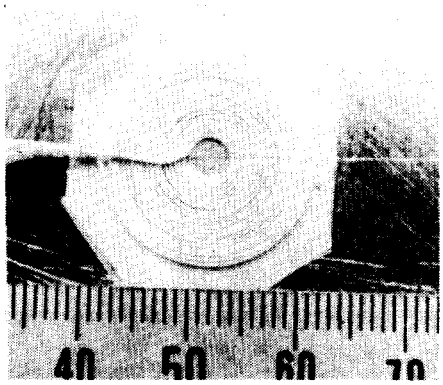

Fig. 7. Flat pancake coil to generate a pulse electromagnetic surface force as a standard ultrasonic wave source.

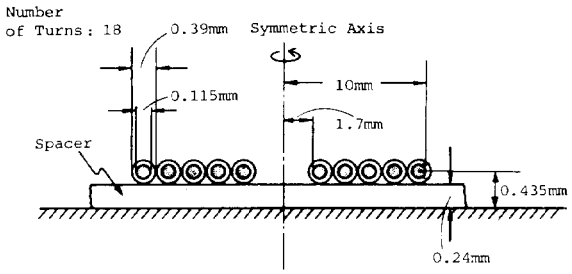

Fig. 8. Schematic cross section of pancake coil.

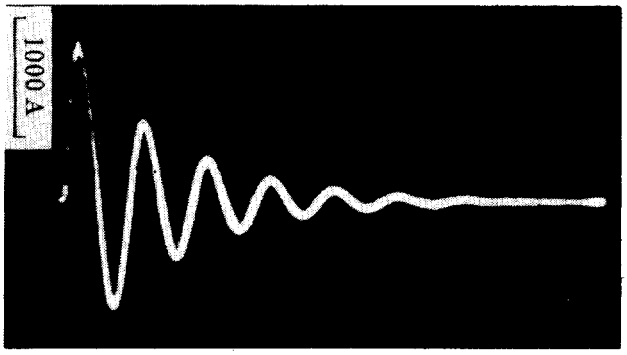

Fig. 9. Pulse current in pancake coil measured by a wide-band current probe.

Because the coil was densely wound in a thin single layer the electromagnetic surface force generated by the coil current is given by substituting the coil conditions and the coil current (22), into (10). The surface force is expressed by (23) and shown in Fig. 12(c)

$$P_P(t) = P_0 e^{-2\alpha t} \sin^2 \beta t, \tag{23}$$

where

$$P_0 = 5.14 \times 10^6 \text{ N/m}^2.$$

$P_P(t)$ works normal to the metal surface in this disc area beneath the coil. There is a small area at the center of the disc area where no surface force exists, but it is small compared with the total disc area and does not have much effect on the ultrasonic wave generation. So, it was assumed that the surface force given by (23) worked uniformly in the disc area, the diameter of which was 20 mm that was equal to the coil's diameter.

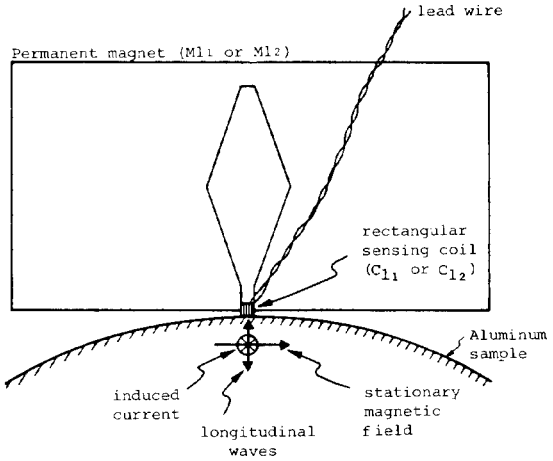

(a)

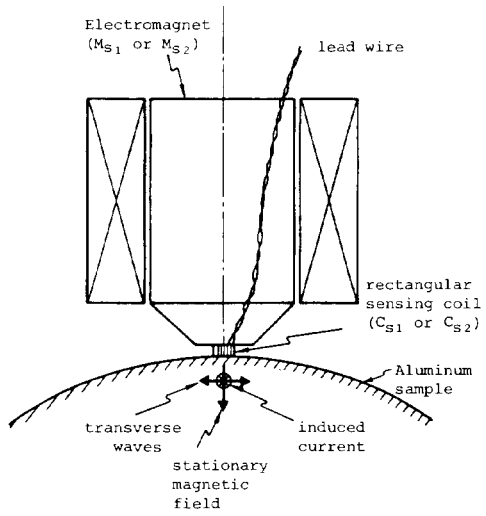

(b)

Fig. 10. Detecting transducers. (a) Dl_1, Dl_2 for detection of normal component of longitudinal wave. (b) Ds_1, Ds_2 for detection of tangential component of transverse wave.

A ceramic transducer connected to an ultrasonic flaw detector (G2N & USIP11: Krautkrämer GmbH) was also used to generate a pulse ultrasonic wave. The effective size of the ceramic transducer was 20 mm in diameter, and the nominal frequency was 2 MHz. It was attached to the same place where the pancake coil was placed and the machine oil was used as an acoustic coupler.

A detecting transducer was put on a point on the curved surface of the metal sample where ultrasonic waves were to be measured. Four detecting transducers were made and used. (See Fig. 10.) The first one of the four detecting transducers Dl_1, is for detection of the normal component of the longitudinal wave. Dl_1 was made from the permanent magnet Ml_1 which produced the stationary magnetic flux of 0.2 Wb/m^2 parallel to the surface of the metal sample, and the small rectangular sensing coil Cl_1 with a base 2 X 2 mm and a height 3 mm. (See Fig. 11.) The magnet wire, 0.1 mm diameter, was used for the coil and the number of turns wound in a single layer was 16. The base area of the coil 2 X 2 mm facing

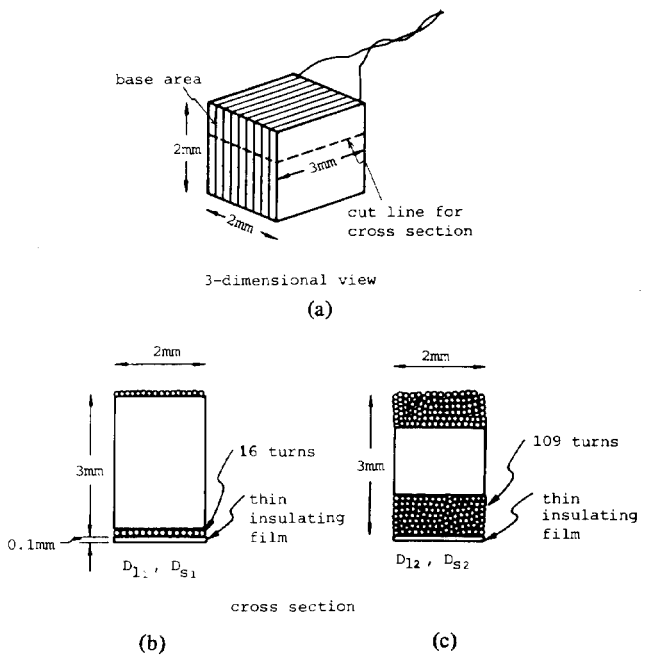

Fig. 11. Rectangular sensing coil. (a) Three-dimensional view. (b) Dl_1, Ds_1. (c) Dl_2, Ds_2.

the surface of the metal sample was covered with a thin insulating film, 0.1 mm thickness. The sum of the insulating thickness 0.1 mm and the one layer wire thickness 0.1 mm is very small compared with the size of the 2 X 2 mm, and so it was assumed that only this base area was effective to detect an ultrasonic wave and that this area was a part of an infinite plane coil, making the one-dimensional theory for detecting an ultrasonic wave shown in Fig. 5 and (21) approximately valid for Dl_1.

The second one is Dl_2, and is also for detection of the normal component of the longitudinal wave. The structure of Dl_2 is the same as Dl_1, except for the stationary magnetic flux 0.18 Wb/m^2 and the number of coil turns 109 in multilayers. This transducer Dl_2 was used in case the higher sensitivity of Dl_1 was necessary. However, it is not advisable to compare directly the experimental results obtained by Dl_2 with the theoretical results, because the total thickness of the multilayers of the rectangular coil Cl_2 is not small compared with the size of the base area of the coil and the one-dimensional theory is not valid any more. To make the comparison possible, the relative sensitivity of Dl_2 to Dl_1 was determined by measuring the same pulse ultrasonic wave by the two transducers, and it was found that the relative sensitivity was 4.1 to 1.

The third one, Ds_1 is used to detect the tangential component of the transverse wave. Ds_1 was made from the electric magnet Ms_1 that produced the stationary magnetic flux of 0.32 Wb/m^2 normal to the surface of the metal sample and the small rectangular coil Cs_1 that was made exactly the same as the coil Cl_1. The fourth one is Ds_2, and it was made for the same reason as Dl_2. The relative sensitivity of Ds_2 to Ds_1 was found to be 7 to 1.

The pulse voltage induced in the detecting transducer was first fed to a unit gain amplifier of a very high input impedance (0032C: National Semi-conductor), then amplified by 40 dB by a wide-band amplifier with 50 Ω input and output impedance (461A: Hewlett-Packard) and displayed on a storage oscilloscope terminated by 50 Ω resistance (7620: Tektronix) which was recorded on a photographic film.

The metal sample used is one-half of an aluminum column, radius 85 mm and height 190 mm. The height is large enough to prevent any unwanted ultrasonic waves reflected at the top and bottom sides of the sample from reaching the detecting transducer earlier than wanted waves. The size of an area on the curved surface of the aluminum sample where detection of ultrasonic waves takes place is considered to be approximately the same as that of the detecting rectangular coil, and it is so small that it can be regarded as a part of a sphere centered by the sound source.

IV. Experimental and Calculated Waveforms

A. Experimental Voltage Waveforms

Four cases of ultrasonic wave pulses were measured every 2°, between 0° and 40°.

1) The normal component of the longitudinal waves generated by the pancake coil was measured by Dl_1. Some of the measured voltage waveforms are shown in Fig. 12(a), A0 ~ A30.
2) The tangential component of the transverse waves generated by the pancake coil was measured primarily by Ds_2 and supplementally Ds_1. Some of the measured voltage waveforms are shown in Fig. 12(b), A4 ~ A30.
3) The normal component of the longitudinal waves generated by the ceramic transducer was measured by primarily Dl_2 and supplementally Dl_1. Some of the measured voltage waveforms are shown in Fig. 13(a), A0 ~ A30.
4) The tangential component of the transverse waves generated by the ceramic transducer was measured primarily by Ds_2 and supplementally by Ds_1. Some of the measured voltage waveforms are shown in Fig. 13(b), A4 ~ A30.

The scale for the vertical axis of Fig. 12(a), A0 ~ A30 which was obtained by Dl_1, has been divided by the amplifier gain 100, in order to show the real induced voltage waveforms in the coil. In the case of Fig. 13(a), A0 ~ A30 which was obtained by Dl_2, the scale has been divided by 100 and then by 4.1, in order to show the voltage waveforms that would have been obtained if Dl_1 had been used instead of Dl_2. In the case of Fig. 12(b), A4 ~ A30 and Fig. 13(b), A4 ~ A30, both of them have been divided by 100 and then by 7.0.

B. Calculated Waveforms

The normal and tangential components of the pulse displacement waveform on a hypothetical sphere radius 85 mm in an infinite elastic half-space were calculated by (11)-(16), using the electromagnetic surface force obtained in the experiment (23) and the physical characteristics of the aluminum sample shown in Table II. The calculated results were multiplied by two to obtain the displacement at the sample surface, on the assumption that the total reflection would take place at the

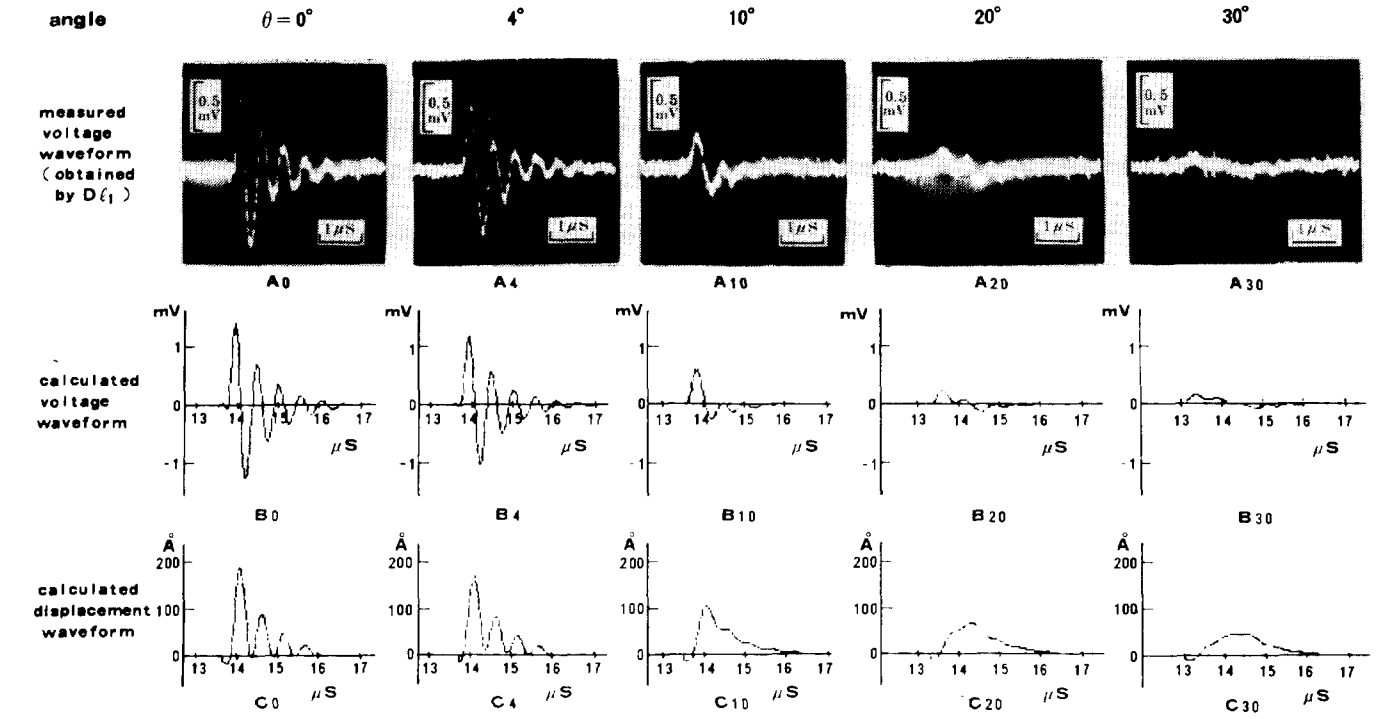

(a)

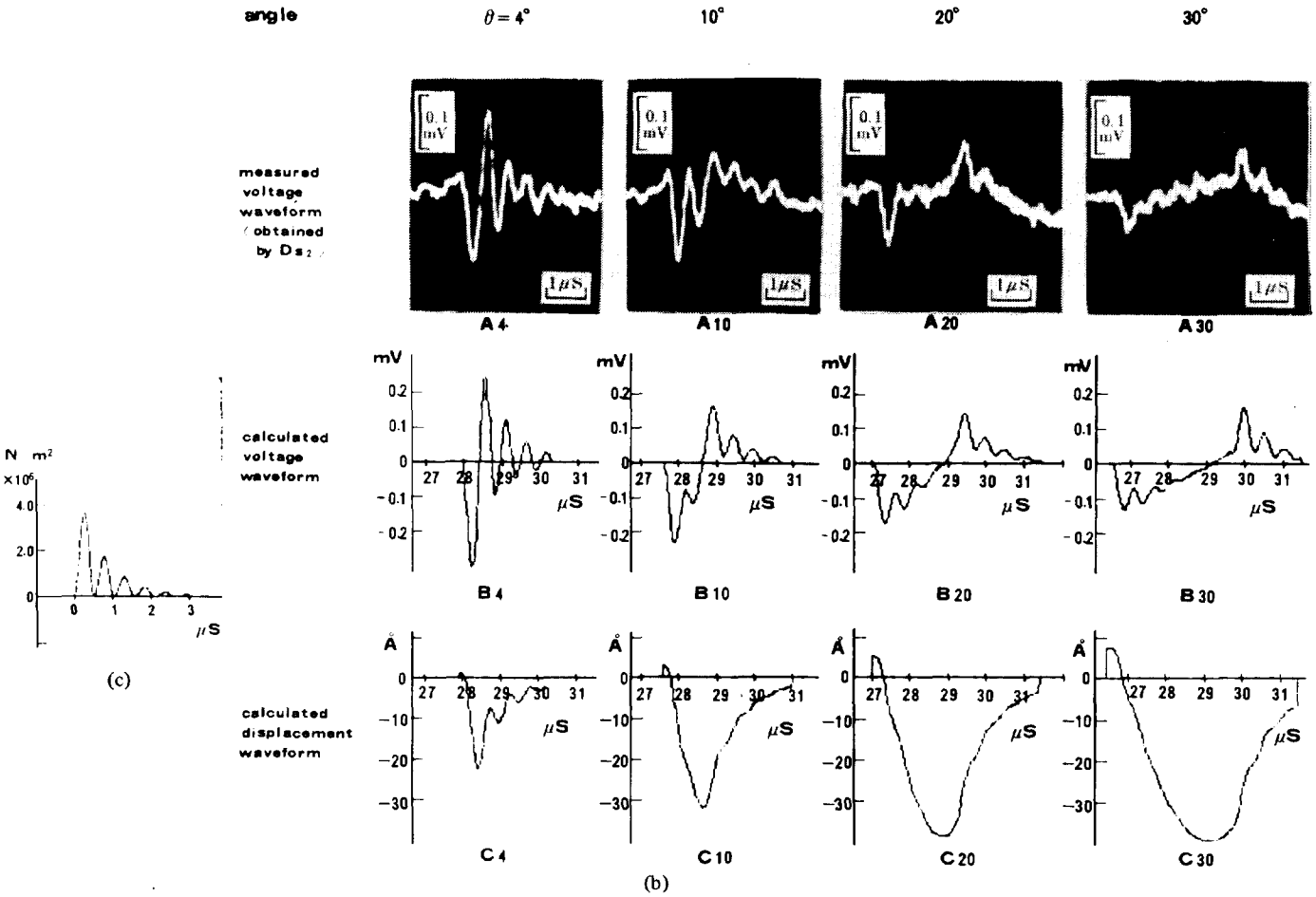

(c)

(b)

Fig. 12. Ultrasonic wave pulses generated by electromagnetic surface force. (a) Longitudinal ultrasonic wave pulses. (b) Transverse ultrasonic wave pulses. (c) Electromagnetic surface force calculated from the observed coil current.

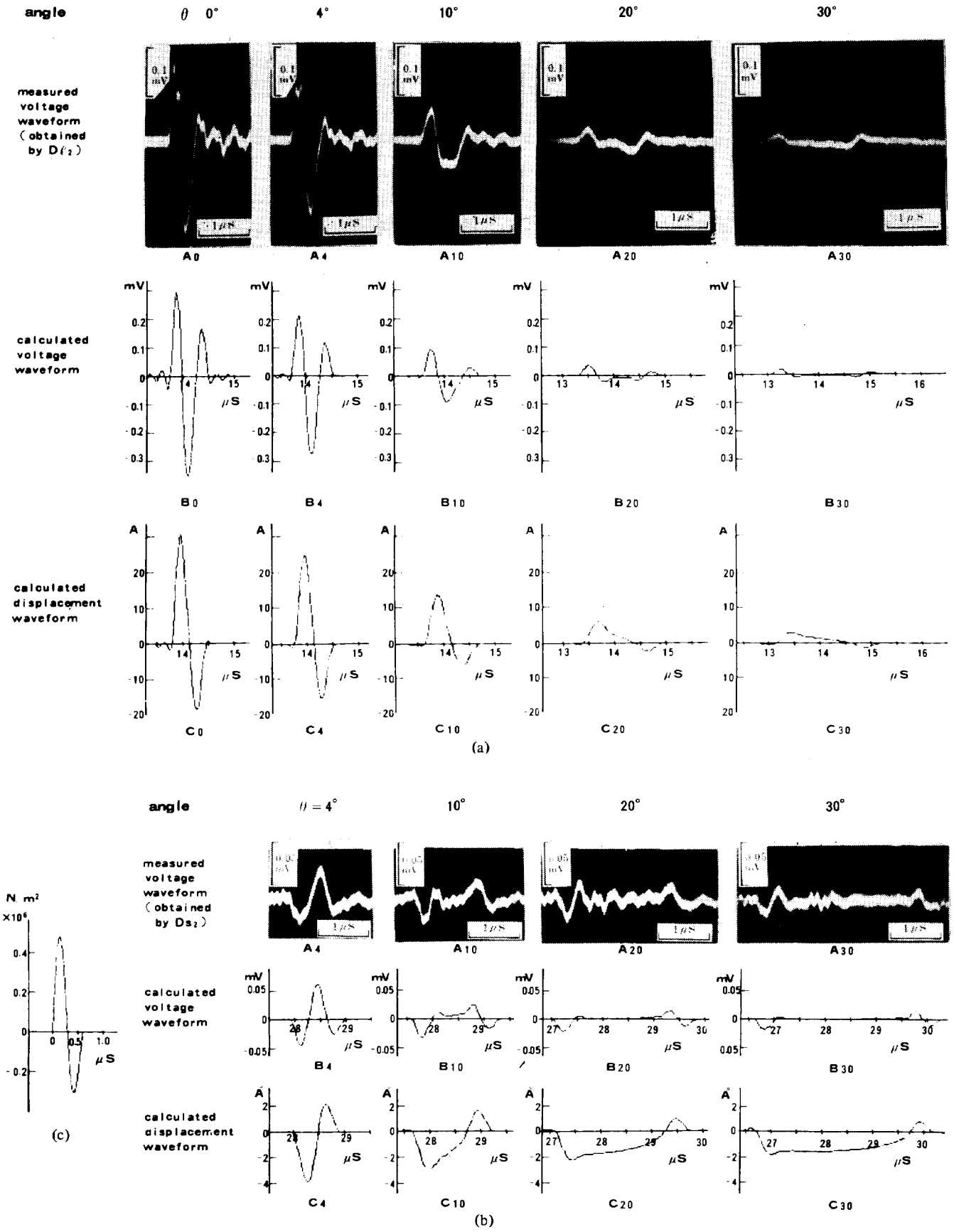

Fig. 13. Ultrasonic wave pulses generated by ceramic transducer. (a) Longitudinal ultrasonic wave pulses. (b) Transverse ultrasonic wave pulses. (c) Hypothetical surface produced by ceramic transducer.

TABLE II
NUMERICAL VALUES USED IN CALCULATION OF ULTRASONIC WAVE PULSES IN ALUMINUM

Quantity	Value
ρ, Density, kg/m^3	2.7×10^3
Lame' constants, kg/m sec^2	
μ	2.561328×10^{10}
λ	5.457996×10^{10}
Wave velocity, m/sec	
longitudinal	6260
transverse	3100
Surface force, N/m^2	
$F_0 e^{-2\alpha t} \sin^2 \beta t$ (electromagnetic surface force generated by the coil)	
F_0	5.14×10^6
α	6.76×10^5
β	5.93×10^6
$F_{C0} e^{-\alpha_C t} \sin \beta_C t$ (hypothetical surface force of the ceramic transducer)	
F_{C0}	7.2×10^5 $0 \le t \le \frac{2\pi}{\beta_C}$
	0 $t<0,\ t>\frac{2\pi}{\beta_C}$
α_C	1.6×10^6
β_C	1.07×10^7
Fourier frequency, MHz	
minimum	0.025
increment	0.025
maximum	5.0
Working Area, m	
radius	10.0×10^{-3}

aluminum-air boundary. The longitudinal and transverse wave pulses were calculated automatically separated in time, because of the difference in velocity between the longitudinal and transverse waves. Such calculations were done every 2°, between 0° and 40°, and some of the calculated displacement waveforms are shown in Fig. 12(a), C0 ~ C30 and Fig. 12(b), C4 ~ C30. Then the displacement waveforms were differentiated with respect to time and multiplied by the sensitivity coefficient of the detecting transducer $N_x W B_0$ 6.4×10^{-3} V s/m, in the case of longitudinal waves, to be detected by Dl_1 and 10.24×10^{-3} V s/m, in the case of transverse waves, to be detected by Ds_1. Some of the calculated voltage waveforms are shown in Fig. 12(a), B0 ~ B30 and Fig. 12(b), B4 ~ B30.

Because the surface force generated by the ceramic transducer was unknown, the hypothetical surface force was determined so that the quantitative difference between the experimental and calculated voltage waveforms was made as small as possible. The resultant hypothetical surface force is expressed by (24) and is shown in Fig. 13(c)

$$F_C(t) = F_{C0} e^{-\alpha_C t} \sin \beta_C t, \quad 0 \le t \le \frac{2\pi}{\beta_C} \tag{24}$$

$$= 0, \qquad t < 0, t > \frac{2\pi}{\beta}$$

where

F_{C0} 0.72×10^6 N/m^2,
α_C 1.6×10^6 1/s,
β_C 1.07×10^7 1/s.

The displacement waveforms and the voltage waveforms were calculated by using the hypothetical surface force (24), and the same method that was used in the case of the electromagnetic surface force. The calculated displacement and voltage waveforms are shown in Fig. 13(a), C0 ~ C30, B0 ~ B30 and Fig. 13(b), C4 ~ C30, B4 ~ B30.

V. COMPARISON AND DISCUSSIONS

The experimental voltage waveforms are very similar to the calculated voltage waveforms for all the cases including the very complicated waveforms seen for the larger angles. (See Figs. 12 and 13.) These results show that the theoretical analysis of the electromagnetic surface force and the characteristics of the detecting transducers are basically correct.

A. Pulse Ultrasonic Waves Generated by the Pancake Coil

The calculated displacement waveform for 0°, in the case of longitudinal waves generated by the pancake coil, Fig. 12(a) C0, resembles the waveform of the surface force Fig. 12(c). This corresponds to the fact that the displacement waveform for 0° in the far field is proportional to the waveform of the surface force, which can be mathematically proven by simplifying (11) for this particular case [7]. The peak height of this waveform is about 200 Å, and it becomes smaller for larger angles, Fig. 12(a) C20, C30, but not as quickly as expected. For example, the peak value for 30°, Fig. 12(a) C30, is about 55 Å which is about a quarter of the peak value for 0°. However, the waveform itself is greatly changed for larger angles, in which the high frequency components are lost and the waveform becomes broader and smoother.

The experimental and calculated voltage waveforms for longitudinal waves, Fig. 12(a) A0 ~ A30 and B0 ~ B30, correspond excellently to each other. The peak height of the voltage waveforms becomes smaller for larger angles more quickly than in the case of the displacement waveform, because the former is proportional to the differentiation with respect to the time of the latter that loses the high frequency component at larger angles. The quantitative peak value of the experimental voltage waveform is about 52 percent of the peak value of the calculated voltage waveform for all the angles. This difference is considered to be caused by several approximations in the theory to calculate the electromagnetic surface force and in the one dimensional theory to calculate the voltage waveform. It is also caused by the unideal experimental conditions, for example, absorption and scattering of ultrasonic waves in the sample and not perfectly uniform stationary magnetic field of the detecting transducers, and other measurement errors. However, this difference is not regarded to be very large considering that this kind of quantitative comparison between the theory and experiment has seldom been done. The measurement reproducibility for the experimental voltage waveform is so excellent that it is possible to

calibrate the detecting transducer just by comparing the experimental and calculated waveforms, and taking account of the absorption and scattering coefficients for the ultrasonic waves in metal.

The peak height of the calculated displacement waveform for 4°, in the case of transverse waves generated by the pancake coil, Fig. 12(b) C4, is about 23 Å, and it grows wider, smoother and bigger for larger angles up to 30° contrary to the case of longitudinal wave. But, this is thought to be inevitably caused by the same waveform of the electromagnetic surface force as is used for a longitudinal wave and the fundamental principles governing wave propagation in the elastic media.

The experimental and calculated voltage waveform, Fig. 12(b) A4 ~ A30 and Fig. 12(b) B4 ~ B30, have complicated waveforms, especially for larger angles, but they agree with each other very well. The peak height of the voltage waveform becomes biggest at about 4° and then becomes smaller for larger angles. The quantitative peak height of the experimental voltage waveform is about 66 percent of the peak height of the calculated voltage waveform for all the angles. This figure 66 percent is not greatly different from the figure 52 percent in the case of longitudinal wave, and the cause of the difference can be explained in the same way.

B. Pulse Ultrasonic Waves Generated by the Ceramic Transducer

The calculated displacement waveforms generated by the hypothetical surface force of the ceramic transducer are much smaller than those generated by the pancake coil, 30 Å at 0° for the longitudinal waves, Fig. 13(a) C0, and about 4 Å at 4° for the transverse waves, Fig. 13(b) C4. Those waveforms become smaller, broader, and smoother for larger angles. It is interesting to know that such a small and fast displacement that is comparable to an atomic scale can be measured by the small electromagnetic-acoustic transducer, because of its time differentiation characteristics. The experimental and calculated voltage waveforms agree with each other very well for all the angles.

C. Pulse Waveform Split

The experimental and calculated waveforms at larger angles for all the cases, for example, Fig. 12(b) A30, B30 and Fig. 13(a) A30, B30 seem to have two independent pulses, but it has been made clear that those are merely produced by differentiation with respect to time of a single displacement waveform whose time duration is long compared to that for smaller angles. Similar phenomena were observed and explained as edge waves [12], [13], but the present results offer a more natural and clearer explanation for this phenomena.

VI. Conclusion

A flat pancake coil with a pulse current is good for a quantitative standard sound source for nonmagnetic metal. The electromagnetic surface force on the metal surface is given by the square of the pulse current in the coil, and the coil dimensions and magnetic permeability of metal.

The electromagnetic-ultrasonic transducer that consists of a small rectangular coil and a magnet is good for quantitative and individual measurement of longitudinal and transverse ultrasonic waves in metal. The pulse voltage waveform induced in the coil is approximately proportional to the differentiation, with respect to time, of a displacement waveform of a pulse ultrasonic wave at the metal surface.

The measured voltage waveforms agreed excellently with the calculated voltage waveforms that were obtained by differentiating, with respect to time, the displacement waveforms calculated by the rigorous integral representations for elastic waves. Quantitative difference between the two waveforms was 48 percent for longitudinal wave and 34 percent for transverse wave. Measurement reproducibility was excellent enabling easy calibration of the transducer.

The pulse waveform split for larger angles was clearly explained by the time differentiation characteristics of the electromagnetic-ultrasonic transducer. Similar phenomena observed earlier by piezoelectric transducers and by the photoelastic visualization methods can be explained in a similar manner.

These results show that both the experimental and calculating methods reported here are good for quantitative evaluation of ultrasonic waves in metal. These methods can also be used for the case of the near field, because no particular method that is valid only for the far field was used. Although the calculating method can only be used for the limited case of a homogeneous semi-infinite elastic half-space, the experimental method, the small electromagnetic-ultrasonic transducer, can be used for all the cases, except for nonlinear magnetic metal and very high frequency ultrasonic waves.

Acknowledgment

The author would like to acknowledge many illuminating suggestions and discussions with Prof. M. Onoe, of the University of Tokyo.

References

[1] L. Filipczynski, "Measurements of longitudinal and transverse waves radiated by a compressional source into elastic semispace," in *Proc. Vibration Problems*, vol. 2, Warsaw, Poland, no. 5, 1964, pp. 85–93.

[2] D. A. Hutchins, R. J. Dewhurst, and S. G. Palmer, "Mechanisms of laser generated ultrasound by directivity pattern measurements," in *Proc. Ultrason. Int. 81*, 1981, pp. 20–128.

[3] W. J. Pardee and R. B. Thompson, "Half-space radiation by EMAT's," *J. NDE*, vol. 1, no. 3, pp. 157–181, 1980.

[4] H. Wüstenberg, "Bestimmung der Richtcharakteristik von Winkelprüfköpfen für die Ultraschallprüfung am Kontrol-körper nach DIN 54120," *Materialprüfung*, vol. 11, pp. 311–315, 1969.

[5] —, "Berührungslose electrodynamische Ultraschallwandler und ihre Vervendung in der Ultrashallprüfung, in *Proc. 6th Int. Conf. NDT, B4*, 1970, pp. 37–48.

[6] H. Nakano, "Some problems concerning the propagations of the disturbances in and on semi-infinite elastic solid," *Geophys. Mag.*, vol. 2, Tokyo, Japan, pp. 189–348, 1930.

[7] G. F. Miller and H. Pursey, "The field and radiation impedance of mechanical radiators on the free surface of a semi-infinite isotropic solid," *Proc. Roy. Soc. London, Ser. A*, vol. 223, pp. 521–541, 1954.

[8] K. Kawashima, "Theory and numerical calculation of the acoustic field produced in metal by an electromagnetic ultrasonic transducer," *J. Acoust. Soc. Amer.*, vol. 60, no. 5, pp. 1089–1099, Nov. 1976.

[9] C. V. Dodd and W. E. Deeds, "Analytical solutions to eddy-current probe-coil problems," *J. Appl. Phys.*, vol. 39, no. 6, pp. 2829–2838, May 1968.
[10] M. Onoe, "An analysis of a finite solenoid coil near a conductor," *Denki Gakkai Zasshi*, vol. 88, Tokyo, Japan, no. 961, pp. 1894–1902, Oct. 1968.
[11] W. Eisenmenger, "Electromagnetische erzeugung von ebenen Druckstössen in Flüssigkeiten," *Acustica*, vol. 12, pp. 185–202, 1962.
[12] J. P. Weight and A. J. Hayman, "Demonstrations of field phenomena of short pulse ultrasonic transducers," *Conf. Evaluation and Calibration of Ultrason. Transducers*, 1977, pp. 24–32.
[13] W. Sachse, N. N. Hsu, and D. G. Eitzen, "Visualization of transducer-produced sound field in solids," *Proc. Ultrason. Symp. IEEE*, 1978, pp. 139–143.

Katsuhiro Kawashima (M'78) was born in Dairen, Japan, on October 25, 1942. He received the Ph.D. degree in engineering from the University of Tokyo, Tokyo, Japan, in 1982.

Since 1968 he has been in Process Technology R&D Laboratory, Nippon Steel Corporation, Tokyo, Japan. He is a Senior Researcher working on research and development of various online measurement methods for steel, especially electromagnetic ultrasonic transducers. From 1973 to 1975 he was in Nondestructive Testing Laboratory, Oak Ridge National Laboratories, Oak Ridge, TN, as a Researcher.

Dr. Kawashima received an Achievement Award from the American Society for Nondestructive Testing in 1977 and the Best Paper Award from the Japanese Society for Nondestructive Inspection, in 1982.

An Investigation of Aging in a Quartz Crystal by VLF Phase Comparison Method

EROL AYGÜN AND ALI ALAÇAKIR

***Abstract*—The objective of the study presented here is the determination of aging characteristics of the local crystal which has been in continuous operation for fifteen years. To do this, the data accumulated since 1968, by phase comparison of the local crystal with the 16 kHz primary standard frequency emitted from Rugby, England, has been analyzed from the point of view of aging in the local crystal. The aging rate, which was parts in 10^9 per day at the very early phase of operation of the local crystal, came down to parts in 10^{12} per day at present. In this study an *AT*-cut rectangular quartz plate vibrating at 5 MHz is used. Since there is not a unique theory of aging in literature for crystal resonators, an attempt to explain the time dependence of the aging rate for the *AT*-cut crystal chips is made by making use of observed aging characteristics. It is believed that the study may help in the developments of nonaging quartz crystal units.**

I. Introduction

THE demand continues forever for greater precision and accuracy in frequency and time measurements in technology. Primary standard frequencies based on atomic standards are being used for frequency and time control or calibration at calibration centers, physical research laboratories, astronomical observatories, missile and satellite tracking stations, radio monitoring and transmitting stations, and manufacturing plants. Local secondary frequency and time standards in such institutions require regular comparisons to a recognized primary standard to maintain their accuracies. At present increased accuracy and increased reliability are inseparable design objectives of designers of high precision electronics.

Atomic standards are being used as the primary reference for comparisons of local standard frequency crystals. Since 1967 the SI definition of the unit of time has been based on the atomic cesium hyperfine transition for which $\Delta\nu$ = 9192.631770 MHz which constitutes a true primary frequency reference [1], [2].

Local quartz crystal oscillators constitute the secondary frequency standards at present. Because crystalline quartz has great mechanical and chemical stability and a small elastic hysteresis, just a small amount of energy is required to sustain oscillations. The linkage of mechanical and electrical effects in quartz crystals is the subject of the piezoelectricity [3].

An oscillating crystal for the frequency standard is characterized by its stabilities; both long-term and short-term. The long-term stability refers to slow changes with time in average frequency. This change arises usually from the aging of the crystal and the long-term stability is also called the aging rate and expressed in parts per unit time. On the other hand, the short-term stability refers to changes in average frequency over a time span sufficiently short that the long-term effects may be neglected. The aging rate of a perfect crystal may be expected to be constant in time at a constant oven setting. But in practice this is not the case, though, after the initial aging period (roughly few months), the rate can be taken to be constant for practical purposes in short enough time intervals.

Manuscript received June 1983; revised December 1983.

E. Aygün is with the Middle East Technical University, Physics Department, Ankara, Turkey.
A. Alaçakir is with the Ankara Nuclear Research and Training Center, Beşevler, Ankara, Turkey.

0018-9537/84/0300-0094$01.00